

Anomalous and planar Righi-Leduc effects in Ni 80 Fe 20 ferromagnets

B. Madon, Do Ch Pham, J.-E. Wegrowe, Daniel Lacour, M. Hehn, V. Polewczyk, A. Anane, V. Cros

▶ **To cite this version:**

B. Madon, Do Ch Pham, J.-E. Wegrowe, Daniel Lacour, M. Hehn, et al.. Anomalous and planar Righi-Leduc effects in Ni 80 Fe 20 ferromagnets. Physical Review B: Condensed Matter and Materials Physics (1998-2015), 2016, 94 (14), pp.144423 (1-8). 10.1103/PhysRevB.94.144423 . hal-01646502

HAL Id: hal-01646502
https://hal.science/hal-01646502

Submitted on 11 Sep 2020

HAL is a multi-disciplinary open access archive for the deposit and dissemination of scientific research documents, whether they are published or not. The documents may come from teaching and research institutions in France or abroad, or from public or private research centers.

L'archive ouverte pluridisciplinaire **HAL**, est destinée au dépôt et à la diffusion de documents scientifiques de niveau recherche, publiés ou non, émanant des établissements d'enseignement et de recherche français ou étrangers, des laboratoires publics ou privés.

Anomalous and planar Righi-Leduc effects in $Ni_{80}Fe_{20}$ ferromagnets

B. Madon, Do Ch. Pham, and J.-E. Wegrowe*
Laboratoire des Solides Irradiés, Ecole polytechnique, CNRS, CEA, Université Paris-Saclay, F 91128 PALAISEAU, France

D. Lacour, M. Hehn, and V. Polewczyk
Institut Jean Lamour UMR 7198 CNRS, Université de Lorraine, Vandoeuvre les Nancy, France

A. Anane and V. Cros
Unité Mixte de Physique, CNRS, Thales, Université Paris-Sud, Université Paris-Saclay, 91767, Palaiseau, France
(Received 14 May 2016; revised manuscript received 9 September 2016; published 19 October 2016)

In this paper, we report experimental evidence of anomalous and planar Righi-Leduc effects on NiFe. The Righi-Leduc effect is the thermal analog of the Hall effect, in which the electric current is replaced by the heat current and the electric field by the temperature gradient. When the material is ferromagnetic, it is well known that there are two other contributions to the Hall voltage which depend on the orientation of the magnetization. These two extra contributions are called the anomalous Hall effect when the magnetization is out of the plane of the sample and the planar Hall effect when the magnetization is in the plane of the sample. In the same way, an anomalous and a planar Righi-Leduc effects are shown to appear when a transverse temperature gradient is generated by a heat current.

DOI: 10.1103/PhysRevB.94.144423

The development of magnetic sensors based on thermoelectric properties has attracted considerable attention in the framework of spin-caloritronics studies. In order to replace the electric generator by heat currents as a power supply for magnetic sensors, it is possible to exploit pure thermomagnetic properties. In this context, the goal of this work is to study the anomalous and planar Righi-Leduc effect of NiFe ferromagnetic layers.

The *Righi-Leduc* effect [1] is the thermal counterpart of the well-known *Hall effect* [2], and it accounts for the temperature gradient developed transversally under a static magnetic field in response to a heat current. In ferromagnetic layers, these effects are qualified as *anomalous*, when the magnetization is perpendicular to the plane of the layer and *planar* when the magnetization is in the plane of the layer. These *anomalous* and *planar* effects, which are related to the magnetization orientation in ferromagnets, are usually much greater than the normal effects which are due to the external field. The case of electric transport is well known, with the anomalous [3,4] and planar [5] Hall effects, but the same anisotropy is also present in the case of thermoelectric transport measurements, in terms of anomalous and planar *Nernst* effects, and in the case of full thermal transport [6].

The anomalous and planar effects are due to the presence of a magnetization, i.e., of an axial vector. Indeed, the application of an axial vector (magnetic field, magnetization, angular velocity, etc.) on an initially isotropic space partially breaks two different symmetries. These symmetries are, on the one hand, the *invariance under time reversal* of the dynamical equations at the microscopic scale [7], and on the other hand, the *rotational invariance*. However, the symmetry break is partial. Indeed, in the first case, the time-reversal invariance is recovered by the application of a π rotation to the magnetization, and in the second case, the symmetry break is partial because the system is still invariant under any rotation around the axis defined by the magnetization. The consequence of these symmetries is to impose a specific form to the transport equations (either electric, thermoelectric, or thermal). This specific form is characteristic of the anisotropic transport [6], whatever the nature of the carriers. From this point of view, the anomalous Righi-Leduc described here (see also Ref. [8]) generalizes to any ferromagnet the so-called magnon Hall effect [9–12] that has been observed on insulating ferromagnets with an intrinsic crystalline chiral structure [13,14]. It also extends the observation of magnetothermal resistance measured in Ni nanowires [15] to ferromagnetic Righi-Leduc effects.

The typical experimental configuration is sketched in Fig. 1. A heat current is injected into the NiFe layer, and the voltage is measured on the transverse metallic electrode. This geometry is the one used in most of the reports about transverse Spin-Seebeck measurements and about anomalous and planar Nernst effects measurements.

We show below that a part of the magnetovoltaic signals measured is due to the anomalous and planar Righi-Leduc effect and neither exclusively to the anomalous and planar Nernst effects as discussed recently [16–22] nor to the so-called spin-Seebeck effect [23]. In order to rule out both the Nernst and the spin-Seebeck contributions, different thermocouple have been used with Pt, Cu, and Bi electrodes.

The paper is composed of four sections. The phenomenology of the anisotropic transport processes is presented in Sec. I. The experimental protocol for thermal injection and the characterization of the system are presented Sec. II. The experimental results are presented in Sec. III, and the conclusion is presented in the last section.

I. ANISOTROPIC TRANSPORT EQUATION

The equations of electric, thermoelectric, and thermal transport in ferromagnetic materials take the same form [6]

*jean-eric.wegrowe@polytechnique.edu

 ©2016 American Physical Society

because of the symmetry of the transport matrix that links the flux to the forces (the so-called Onsager matrix). Indeed, the time-reversal invariance of the microscopic equations and the rotational symmetry of the system around the magnetization direction are valid whatever the type of carriers involved (electron, phonon, magnon, etc.).

In the case of electric transport, the generalized Ohm's law is well known [5]:

$$\vec{\mathcal{E}} = \rho\, \vec{J}^e + \Delta\rho(\vec{J}^e.\vec{m})\vec{m} + \rho_{AH}\, \vec{m} \times \vec{J}^e, \qquad (1)$$

where $\vec{m}$ is the magnetization orientation, $\vec{\mathcal{E}}$ is the electric field, $\vec{J}^e$ is the electric current, ρ is the electric resistivity of the ferromagnetic layer, $\Delta\rho$ is the anisotropic magnetoresistance (AMR), and ρ_{AH} is the anomalous Hall resistivity.

The generalized Fourier law which relates the heat current to the temperature gradient takes the same form [6]:

$$\vec{\nabla}T = r\, \vec{J}^Q + \Delta r(\vec{J}^Q\vec{m})\vec{m} + r_{ARL}\, \vec{m} \times \vec{J}^Q, \qquad (2)$$

where $\vec{\nabla}T$ is the temperature gradient, $\vec{J}^Q$ is the heat current density, r is the thermal resistivity, Δr is the anisotropic magnetothermal resistance [15], and r_{ARL} is the anomalous Righi-Leduc coefficient. This equation [so as Eq. (1)] can be recast under a matrix form for a Cartesian basis $\{\vec{e}_x,\vec{e}_y,\vec{e}_z\}$:

$$\vec{\nabla}T = \begin{pmatrix} r+\Delta r\, m_x^2 & \Delta r\, m_x m_y - r_{ARL}\, m_z & \Delta r\, m_x m_z + r_{ARL}\, m_y \\ \Delta r\, m_x m_y + r_{ARL}\, m_z & r+\Delta r\, m_y^2 & \Delta r\, m_y m_z - r_{ARL}\, m_x \\ \Delta r\, m_x m_z - r_{ARL}\, m_y & \Delta r\, m_y m_z + r_{ARL}\, m_x & r+\Delta r\, m_z^2 \end{pmatrix} \vec{J}^Q, \qquad (3)$$

where $\vec{m} = m_x\vec{e}_x + m_y\vec{e}_y + m_z\vec{e}_z$. Using the angular coordinates $\{\theta,\varphi\}$ for the magnetization (Fig. 1), we have $m_x = \cos\varphi\sin\theta$, $m_y = \sin\varphi\sin\theta$, and $m_z = \cos\theta$. The diagonal coefficients account for the anisotropic magnetotransport, while the nondiagonal coefficients account for the anomalous and planar Righi-Leduc effects.

Similarly, at zero electric current ($\vec{J}^e = 0$), and once again for the same symmetry reasons, the thermoelectric transport equation takes the same form [6]: $\vec{\mathcal{E}} = \bar{\bar{S}}_F\vec{J}^Q$ where $\bar{\bar{S}}_F$ is the Seebeck tensor, defined by the Seebeck coefficients S_F and S_{Fz}, and the anomalous Nernst coefficient N_a:

$$\bar{\bar{S}} = \begin{pmatrix} S_F & N_a & 0 \\ -N_a & S_F & 0 \\ 0 & 0 & S_{Fz} \end{pmatrix}. \qquad (4)$$

We then have, like for Eqs. (1) and (2),

$$\vec{\mathcal{E}} = S_F\, \vec{\nabla}T + \Delta S_F(\vec{\nabla}T\vec{m})\vec{m} + N_a\, \vec{m} \times \vec{\nabla}T, \qquad (5)$$

where $\Delta S_F = S_{Fz} - S_F$. Accordingly, the thermoelectric voltage is the same function of the angles θ and φ as the temperature gradient in Eq. (3). This is the reason why it is experimentally difficult to discriminate between the anomalous and planar Righi-Leduc and anomalous and planar Nernst effects measured on conducting ferromagnets. In the experiments in which the temperature difference ΔT_y is measured by a thermocouple (leading to a voltage ΔV_y), the main difference between the two effects is that the anomalous and planar Nernst effects are produced inside the ferromagnetic layer so that the electrode does not play any role. In contrast, for the anisotropic Righi-Leduc effects (also produced inside the ferromagnet), the electrode plays a fundamental role as it converts the temperature difference to a voltage difference. The amplitude of the signal is proportional to the amplitude of the thermocouple. Note also that the thermocouple technique is very efficient when the electrode is thin enough (see below).

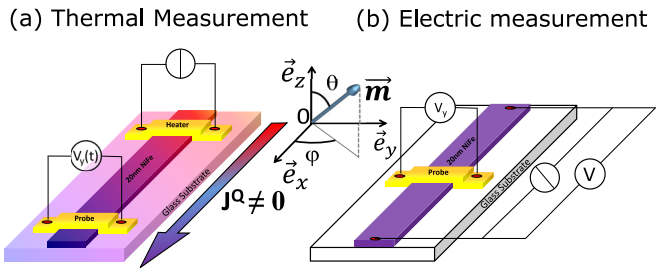


FIG. 1. Schematic views of a typical NiFe device for (a) the anomalous and planar Righi-Leduc effect. The electrode and the heater have a width of 400 μm and are spaced 5 mm apart. (b) Measurements of the anomalous and planar Hall effect and anisotropic magnetoresistance. The magnetization vector $\vec{m}$ is defined by the angles θ and φ. Similarly, θ_H and φ_H define the orientation of the external magnetic field orientation.

II. MAGNETIC, MAGNETOVOLTAIC, AND THERMAL CHARACTERIZATIONS

A. Magnetic characterization

The ferromagnetic layer is a $d_{NiFe} = 20$-nm-thick, 400-μm-wide $Ni_{80}Fe_{20}$ thin film (see Fig. 1) and the probe electrodes (Cu, Pt, Bi) have been fabricated using shadow masks in a sputtering deposition system without breaking the vacuum. The ferromagnetic layer is first deposited on a glass substrate. All the measurements have been done at room temperature, using an electromagnet which provides a magnetic field of $1T$.

As shown below, the magnetization of the permalloy ($Ni_{80}Fe_{20}$) layer is single domain. As a consequence, the magnetization $\vec{M} = M_s\vec{m}$ is a vector of constant modulus M_s (magnetization at saturation) oriented along the unit vector $\vec{m}$ (see Fig. 1). In this study, the magnetization $\vec{m}$ is rotated over the whole configuration space, i.e., over the coordinates θ,φ with the help of the external magnetic field $\vec{H}$ of amplitude H and oriented in the direction (θ_H,φ_H). Two configurations were used. The first one that we will call in-plane configuration (IP) is obtained by varying the azimuthal angle φ_H while keeping the polar angle θ_H fixed to 90°. The second is the out-of-plane configuration (OOP) that corresponds to the change of the polar angle θ_H keeping φ_H fixed to 90° (see Fig. 1 for the

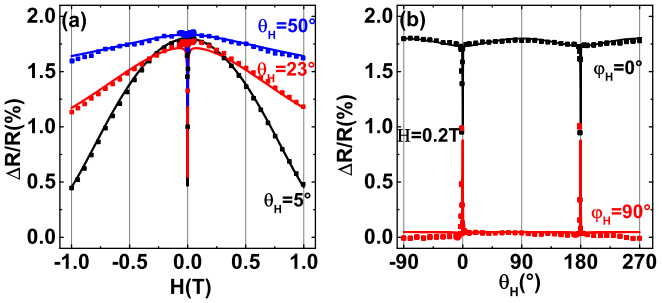


FIG. 2. (a) Magnetoresistance as a function of the amplitude of the external perpendicular field at $\varphi = 0$ for (a) $\theta = 5°, \theta = 23°$, and $\theta = 50°$. The points correspond to the measured data and the line is the fit calculated from the minimization of the magnetic energy F. (b) Magnetoresistance as a function of the out-of-plane angle θ_H for a weak external magnetic field $H = 0.2T$ at $\varphi_H = \varphi = 0°$ (upper curve) and $\varphi_H = \varphi = 90°$ (lower curve).

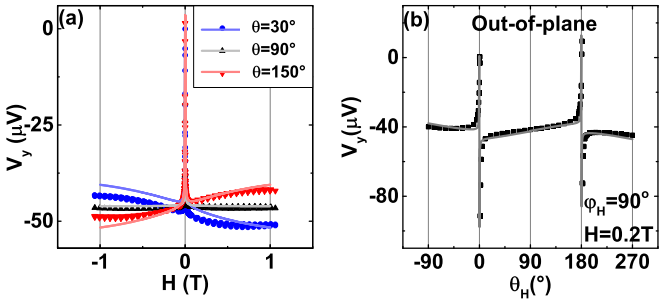


FIG. 3. Anomalous Hall measurement with Cu (5 nm) / Pt (10 nm) as a function of (a) the amplitude of the magnetic field H for different out-of-plane angles and (b) the radial angle θ_H for an applied field of $H = 0.2$ T. The lines correspond to the calculation of the magnetic states.

definition of the angles). The angle is controlled by a rotation around the axis perpendicular to the fixed magnetic field generated by the electromagnet. The different sample holders are used for the two configurations (IP measurements and OOP measurements).

The relation between the magnetic field $\vec{H}$ (i.e., H,θ_H,φ_H) and $\vec{m}$ is given by the minimization of the ferromagnetic free energy. This energy depends on three parameters, namely the magnetization at saturation M_s, the demagnetizing field H_d, and the magnetocrystalline anisotropy field $\vec{H}_{an}$, confined in the plane of the layer. The corresponding energy $\mathcal{F}$ is the sum of the three terms: $\mathcal{F} = -\vec{H}\vec{M} + H_{an}M_s \sin\zeta_a/2 + H_d M_s \cos^2\theta$, where $\zeta_a = (\vec{H}_{an},\vec{m})$ is the angle between the magnetocrystalline anisotropy axis and the magnetization, and θ is the angle between the vector $\vec{n}$ normal to the plane of the layer and the magnetization. The minimum is calculated through numerical methods (MATHEMATICA program). The magnetization states were characterized using anisotropic electric transport properties, on the basis of three different experimental configurations [see Fig. 1(b)] contained in Eq. (1), which correspond to anisotropic magnetoresistance (AMR), planar Hall effect (PHE), and anomalous Hall effect (AHE).

For AMR measurements, the voltage is measured along the same axis as the current flow [see Fig. 1(b)]. Figure 2 shows the magnetoresistance as a function of the external magnetic field at $\varphi = 0°$ for three different angles [Fig. 2(a)] and as a function of the out-of-plane angle θ_H [Fig. 2(b)] for a weak magnetic field of $0.2T$. The fitted parameters are $H_d = 1T$ and the AMR ratio is found to be $\Delta R/R = 1.83\%$. Note that the saturation is not reached for $H = 1T$. Consequently, the direction of the magnetization (θ,φ) does not exactly coincide with that of the external field (θ_H,φ_H). This characteristic will be exploited in Sec. III below in order to show that the magnetovoltaic signal is not a response to the external magnetic field but is a response to the magnetization. The second striking result is the jump at low field, if the magnetization is closed enough to the normal of the layer. This causes an sharp irreversible jump from the near out-of-plane configuration at $\varphi = 0$ to the in-plane configuration of angle $\varphi \neq 0$ corresponding to the direction of the small anisotropy in the plane. The jump of the magnetization occurs when the projection of the external field does no longer compensate for the anisotropy field in the plane.

Figure 3 shows the anomalous Hall measurements which appears when an electric current is set between the two end of the NiFe layer. It is easy to recognize the different magnetic configurations identified above.

B. Experimental protocol and thermal characterization

An AC electric current $I(t) = I_0\cos(\omega t)$ is injected into the heater electrode of resistance R in order to produce a heat current $J_x^Q(t) = cRI_0^2[\cos(2\omega t) + 1]/2$ at the level of the probe electrode, having twice the pulsation of the electric current. The power $P = RI(t)^2$ injected is of the order of a fraction of 1 W. The parameter c, defined by the relation $J_x = cP$, is a constant which links the heat current density to the injected power. It has the dimension of the inverse of a surface and takes into account all the losses in the surrounding environment. This parameter changes from one sample to the other but it is typically of the order of 1 mm^{-2}, and has been studied by numerical simulations. The voltage is then recorded over time on a second electrode 5 mm away from the heater. Figure 4 shows a typical measurement of this voltage. It is composed of a DC offset, a small ω voltage, and a 2ω voltage $V_y^{2\omega}$. The 2ω voltage is the voltage of interest in this study and is the response to the heat excitation applied to the sample only.

We checked that the amplitude of the magnetovoltaic signal is proportional to the averaged power P injected in the heater. Figure 5(a) shows the 2ω voltage $V_y^{2\omega}$ defined in Fig. 4 as a function of the averaged power. The voltage is measured for three orientations of the magnetization: two perpendicular to the plane $\theta = 0°$ and $\theta = 180°$, and one in the plane $\theta = 90°$. We define $\delta(\Delta V_y)$ as the 2ω-voltage maximum difference as a function of the magnetization state. The magnetovoltaic signal $\delta\Delta V_y(P)$ allows us to select the contributions due to *the heat carriers that are correlated to the ferromagnetic degrees of freedom* (e.g., magnons). The other thermally induced contributions are isotropic and do not play any role in the signal $\delta(\Delta V_y)$ of interest. It can be seen that, in a first approximation, the magnetovoltaic signal $\delta(\Delta V_y)(P)$ is linear in P, so that the coefficient c does not depend on the power injected.

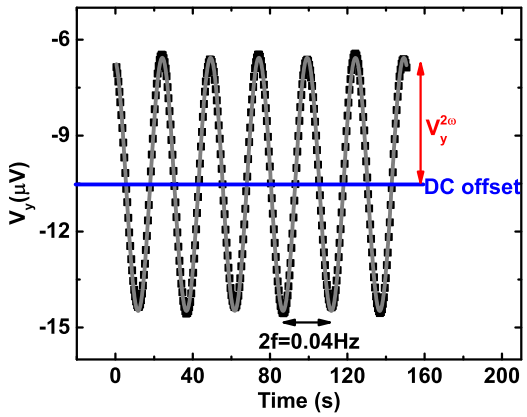


FIG. 4. Time dependance of the transverse voltage for a 50-nm Pt electrode. The modulation frequency is $2f = \omega/\pi = 0.04$ Hz. The external field is 1 T and is applied along $\theta_H = 0$, which is perpendicular to the sample plane. We define $\Delta V_y = V_y^{2\omega} - V_0^{2\omega}$ where $V_0^{2\omega}$ is the 2ω voltage measured without external magnetic field.

Next, we studied the influence of frequency on the voltage. Figures 6(a) and 6(b) allow us to compare V_0, which is the $V_y^{2\omega}$ voltage at zero external field, and $\delta(\Delta V_y)$ as a function of the square root of the frequency of the power injected in the heater. We find that the frequency window of interest is in the range 10^{-2} to 5×10^{-2} Hz. Below this value, the other parts of the system start to play an important role. Above this value, the proportion J_x^Q of the heat current that flows inside the ferromagnetic layer along the $\vec{e}_x$ direction is no longer sufficient to keep a sufficiently large signal-to-noise ratio. Using a very simple one-dimensional (1D) infinite rod model to solve the Fourier equation we could extract the diffusivity which corresponds to Figs. 6(a) and 6(b). For Fig. 6(a), which is the 0 field 2ω voltage, we found a value smaller than for Fig. 6(b), which is the magnetization-dependent 2ω voltage. This confirms that $\delta(\Delta V_y)$ is the response to the heat which flows inside the permalloy layer. This 1D model also explains the reason why we used a smaller frequency that the one used elsewhere in the literature for similar technics. Indeed, in this model, the voltage decays exponentially with distance and our electrode is millimeters away from the heater, which is several order of magnitude farther than in Refs. [24,25].

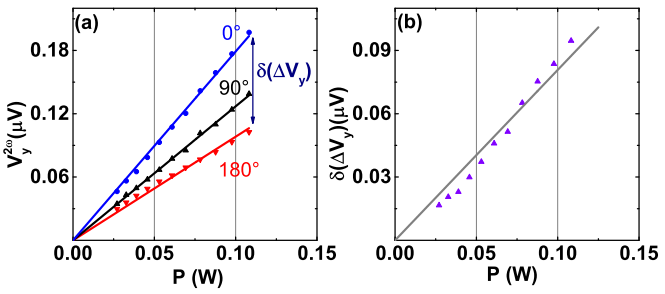


FIG. 5. (a) Measurement of the voltage $V_y^{2\omega}$ as a function of the heat power injected for different values of the out-of-plane applied field. (b) Magnetothermal response $\delta(\Delta V_y) = \Delta V_y(\theta = 0^\circ) - \Delta V_y(\theta = 180^\circ)$ as a function of the power injected.

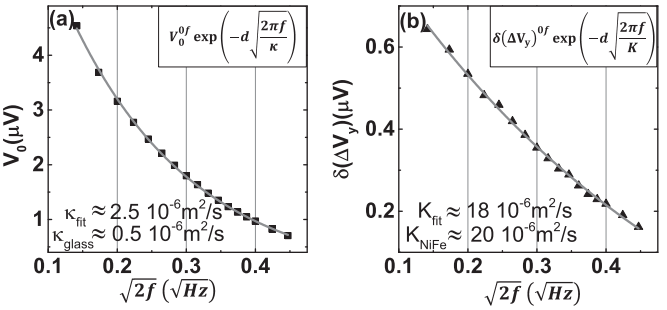


FIG. 6. (a) Thermoelectric voltage at 0 field, V_0, and (b) magnetovoltaic signal $\delta(\Delta V_y)$ (as defined in the caption of Fig. 5) as a function of the square root of the freqency $\sqrt{2f}$. The squares are the experimental data and the gray line is the exponential relaxation with the adjustable thermal diffusivities κ (a) and K (b) that are compared to the known values.

From this study, we can conclude that a 1D model allows us to understand the frequency dependence of the 2ω voltage. We can then assume that the heat current is mainly flowing along the $\vec{e}_x$ direction. This will be confirmed by the characterization of the thermocouples below and by the observed angular dependence in the next section.

C. Probe electrode as thermocouple

In order to measure the anisotropic thermal transport described by Eq. (3), a thin metallic electrode is deposited on the ferromagnet, which plays the role of thermocouple. This thermocouple is composed of three parts: the electrode (Pt, Cu, or Bi), the ferromagnetic layer, and the electric wires that connect the electrode to the rest of the circuit. We call this probe thermocouple ΔS_{tc}. In the ideal thermocouple, ΔS_{tc} is simply the difference between two Seebeck coefficients of the materials that compose the interface, but this expression is more complicated in general. In order to measure the parameter ΔS_{tc} independently, we used the electrodes (Cu, Pt, or Bi) deposited on the ferromagnet and contacted to aluminum wires by silver paint.

The thermoelectric voltage was measured over time while diving one side of the probe electrode in an ice-water bath. The other side of the electrode is kept at room temperature. This arrangement imposes a maximum temperature difference of about $\Delta T \approx 15.6^\circ$. The fit of the time decay allows us to corroborate the analysis of the thermal regime performed in the previous subsection (Fig. 6). The maximum difference $\Delta U_{tc}(t)$ is a measure of the thermocouple ΔS_{tc} (V/K). Figure 7 shows that the NiFe-Al interface has a strong and negative ($-16.2\ \mu$V/K) contribution to ΔS_{tc}, while Cu and Pt give a small and positive contribution ($<1\ \mu$V/K). As a consequence, NiFe gives a higher contribution to the thermocouple than Pt and Cu and the total thermocouple is negative and of the order of $-10\ \mu$V/K.

The values of the thermocouples show that a voltage difference of $\Delta V_y \approx 0.1\ \mu$V corresponds to a temperature difference of the order of 6×10^{-3} K. This voltage is amplified considerably by the use of a Bi electrode, for which ΔS_{tc} is nearly two order of magnitudes higher.

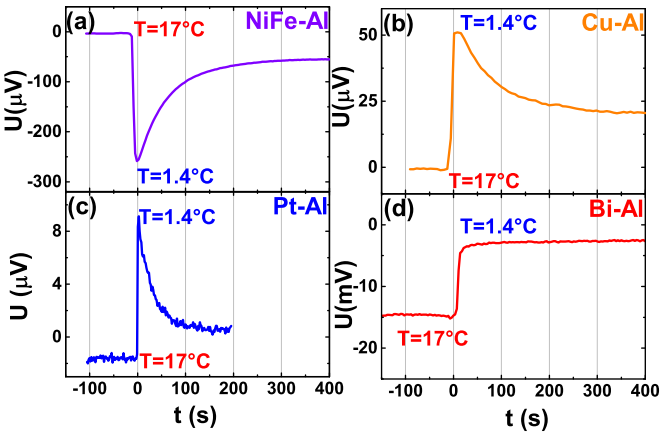


FIG. 7. Thermoelectric voltage generated by a contact wire of Al on (a) NiFe (Py), (b) Cu, and (c) Pt, (d) Bi as a function of time. The temperature difference of $\Delta T = 15.6^{o}$ is imposed at $t = 0s$, then the metallic electrode thermalizes to a steady state temperature gradient.

In conclusion, the temperature difference ΔT_y generated perpendicular to the heat flow between the two edges of the ferromagnetic layer can be measured thanks to the probe thermocouple. In the case of the anomalous and planar Righi-Leduc effect, if the heat current flows along the $\vec{e}_x$ direction, the signal follows the equation given by the first term of the second line in the matrix of Eq. (3):

$$\Delta V_y \approx J_x^Q \Delta S_{tc} \left[\frac{\Delta r}{2} \sin(\theta)^2 \sin(2\varphi) + r_{ARL} \cos(\theta) \right] \quad (6)$$

The second term in the right-hand side of Eq. (6)—proportional to $\cos(\theta)$—defines the anomalous Righi-Leduc coefficient r_{ARL} of the ferromagnet, that can be measured directly with setting $\varphi = 0^\circ$ or $\varphi = 90^\circ$ (out-of-plane measurements). On the other hand, the first term in the right-hand side of Eq. (6) proportional to $\sin(2\varphi)$ defines the planar Righi-Leduc coefficient Δr of the ferromagnet, that can be measured directly with setting $\theta = \pi/2$ (in-plane measurements).

III. EXPERIMENTAL RESULTS

A. Magnetovoltaic signal

Figure 8 shows the signal $\Delta V_y = V_y^{2\omega} - V_0^{2\omega}$ measured on a Pt electrode (where $V_0^{2\omega}$ is the signal without applied magnetic field) as a function of the angle of the external field. The first point to notice is that in the IP configuration the signal is π periodic [Fig. 8(a)] whereas in the OOP configuration it is 2π periodic [Fig. 8(b)]. The second thing is that for the OOP configuration the angular dependance has a triangular shape [Fig. 8(b)]. The periodicity can be easily understood from Eq. (6). In the IP configuration, Eq. (6) gives a $\sin 2\varphi$ angular dependence while in the OOP configuration we expect a $\cos\theta$ angular dependence. It is important to notice that the angles θ and φ in Eq. (6) describe the magnetization and not of the magnetic field (θ_H and φ_H). For the IP configuration, they are the same as for a 1T magnetic field $\varphi_H = \varphi$ but in the OP configuration $\theta_H \neq \theta$. The gray line is obtained after calculating the value of θ as a function of θ_H using the characterization and analysis present in Sec. II A.

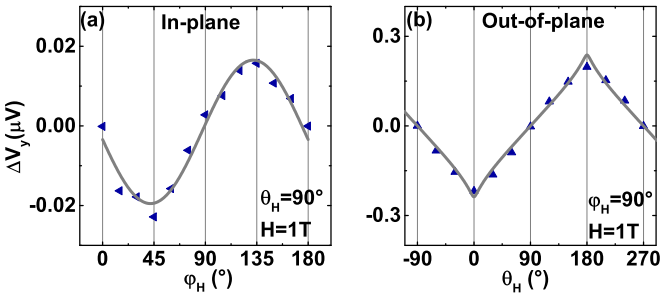


FIG. 8. Transverse voltages $\Delta V_y =$ as a function of the direction of the $1T$ magnetic field H. (a) In-plane configuration for which the polar angle θ_H is fixed and equal to 90°, the azimuthal angle φ_H is varied (◀); (b) out-of-plane configuration for which the azimuthal angle φ_H is fixed to 90° and the polar angle is varied (▲).

Figure 9(a) shows the thermomagneto-voltaic signal ΔV_y as a function of the applied magnetic field for Pt electrodes, and Fig. 9(b) displays the OOP angular dependence for a relatively weak external magnetic field. These signals have both an anomalous and a planar contribution. At high field the difference between −1 T and 1 T originates from the out-of-plane component of the magnetization whereas at low field a peak is observed and is due to the small uniaxial anisotropy mentioned in Sec. II A. Figure 9(b) shows the irreversible jump of the magnetization into the plane, as a signal superimposed to the typical anisotropic signal of Fig. 8(b). As shown in the analysis of Sec. II A and Fig. 3, the jump of the magnetization is expected to be due to the anisotropy field in the plane of the layer. This feature is well reproduced by the numerical calculation with a uniform magnetization state (continuous lines from Figs. 8 to 11).

The differences that can be observed between the anomalous and planar Hall effect shown in Fig. 3 and the anomalous and planar Nernst or anomalous and planar Righi-Leduc shown in Fig. 9 are due to the relative amplitude of the anomalous and planar coefficients. In the case of electric current the planar coefficient is much larger than the anomalous coefficient and it is the exact opposite in the case of thermal current. This observation may be of interest and could shed light on the microscopic origin of the Righi-Leduc coefficients in forthcoming studies.

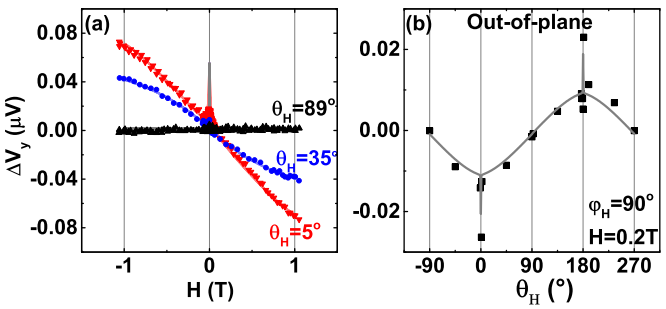


FIG. 9. Transverse voltage ΔV_y on a Cu (5 nm)/Pt (10 nm) electrode as a function of (a) the amplitude of the magnetic field H for three out-of-plane angles and (b) the radial angle θ_H for an applied field of $H = 0.2$ T. The gray line corresponds to the calculation of Eq. (6).

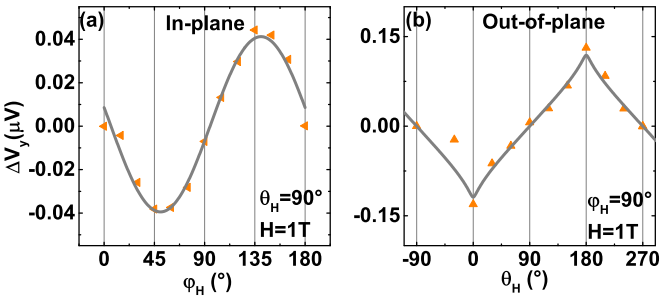


FIG. 10. Transverse voltage ΔV_y for a 20-nm Cu probe electrode as a function of (a) the in-plan angle φ_H and (b) the out-of-plane angle θ_H.

At this stage, we showed that the voltage measured on the transverse electrode when a heat current is injected depends on the orientation of the magnetization (and not of the magnetic field), and that it follows the typical symmetries of the anisotropic transport equations. However, as stated in Sec. I, it is impossible to distinguish the anomalous and planar Nernst effect from the anomalous and planar Righi-Leduc effect using only symmetry considerations. Consequently the next step investigates the influence of the material of the electrode on this voltage.

B. Nature of the electrodes

Figure 10 shows the results obtained on a device in which the Pt probe electrode is replaced by a Cu electrode (99.9999% purity target). The observation of the same magnetovoltaic signals for both electrodes rules out the spin-Seebeck interpretation, which is based on the hypothesis on inverse spin Hall effect (ISHE). Indeed, since there is no sizable spin-orbit coupling, the ISHE effect is absent in Cu [26–28]. Furthermore, the π periodicity of the planar signal is not compatible with the 2π periodicity expected in the case of spin-Seebeck interpretation.

However, the comparison between Pt and Cu electrodes does not allow us to conclude about the role of the thermocouple because the thermocouples have comparable order of magnitude. But if the same experiments are performed on a device in which the probe electrode is replaced by a 200-nm Bi electrode, the amplitude of the signal is amplified by a factor of 10, as shown in Fig. 11. Note that only the IP measurements have been shown in Fig. 11 because the OOP measurements are largely dominated by the direct Nernst voltage of the Bi electrode.

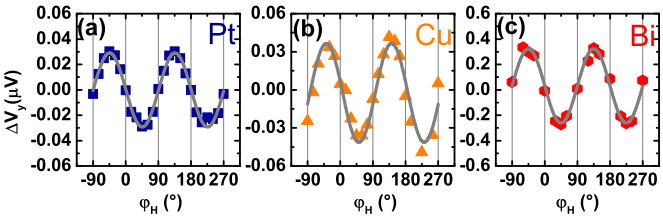


FIG. 11. Transverse voltage ΔV_y vs φ_H for in-the-plan configuration with (a) Pt, (b) Cu, and (c) Bi electrodes. The signal with Bi electrode is 10 times higher than that with Pt and Cu electrodes.

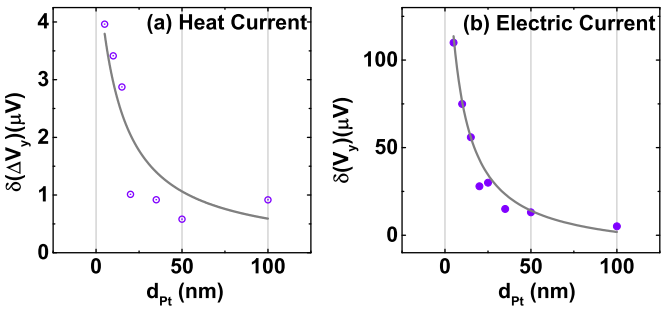


FIG. 12. (a) Maximum out-of-plane voltage response $\delta(\Delta V_y)$ to the thermal excitation J_x^Q vs thickness of the Pt electrode. (b) Electrical counterpart of $\delta(\Delta V_y)$, i.e., the voltage response to the electric excitation J_x^e vs thickness of the Pt electrode (anomalous Hall effect). The gray line presents the expected dependence taking into account only the shunt effect.

Since in the case of the planar Nernst effect the electrode does not play any role, the amplification of the signal observed can only be attributed to the planar Righi-Leduc effect. This observation leads us to conclude that the heat flow J_x^Q generates a transverse temperature difference $\Delta T_y \approx 10\,\mathrm{mK}$, which is by definition the planar Righi-Leduc effect.

The corresponding *anomalous and planar Righi-Leduc* coefficients have been estimated with the help of a numerical study for the evaluation of the heat current J_x^Q (more precisely the coefficient c) at the point of the measurement. In the case of NiFe ferromagnet we obtain $r_{ARL}^{Py} \approx 5\,10^{-2}\mathrm{Km/W}$ for the anomalous Righi-Leduc coefficient and $\Delta r^{Py} \approx 10^{-2}\mathrm{Km/W}$ for the planar Righi-Leduc coefficient. Note that a correction due to respectively anomalous and planar Nernst effects may be necessary for the above coefficients. The anomalous and planar Nernst signals should indeed be expected in the metallic structures [16–22].

C. The role of the thickness of the electrodes

For completeness we checked the effect of the thickness electrode on the transverse voltage measured for both an electric current and a thermal current. We have fabricated several devices having different Pt thickness ranging from 5 to 100 nm. Defining the maximum amplitude of the magnetovoltaic signal $\delta(\Delta V_y)$ as shown in Fig. 5, a decrease of $\delta(\Delta V_y)$ as a function of the probe thickness is observed [Fig. 12(a)]. Such a decrease is often interpreted as the effect of spin injection at the interface [29–31]. Here we demonstrate that the thermal shunt effect suffices to explain the data. Indeed, at the level of the probe electrode, not all the heat current flowing at the level of the probe electrode contributes to the effective current since a part is also flowing into the nonferromagnetic electrode of Pt, Cu, or Bi. Assuming a simple scheme of two thermal conductors in parallel, the effective part of the heat current $J_x^Q(d)$ depends on the thickness d of the electrode, according to the relation

$$J_x^Q(d) = \frac{\rho_{Th}^{Pt} d_{NiFe}}{\rho_{Th}^{Pt} d_{NiFe} + \rho_{Th}^{NiFe} d} J_x^{*Q}. \tag{7}$$

The dependence of the signal on the thickness d of the Pt probe is fitted using the tabulated values $1/\rho_{Th}^{Py} =$

72 W m^{-1} K^{-1} for $Ni_{80}Fe_{20}$ and $1/\rho_{Th}^{Pt} = 46$ W m^{-1} K^{-1} for Pt. The scattering of the experimental points in Fig. 12(a) is due to the variation of the parameter c (accounting for the heat dissipation) from one sample to the other. The gray line is calculated by taking the average of the seven values of the parameter ΔScr_{ARL}, fitted from the angular dependence of each sample [see, e.g., the gray line in Fig. 8(b)]. From the good agreement between the experimental points and the calculated profile in Fig. 12(a), we conclude that the thermal shunt effect is enough to explain the signal decrease as a function of thickness. As shown in Fig. 12(b), this behavior is the exact counterpart of that of the anomalous Hall effect [32] measured on the same sample (see Fig. 3), for which the heat current $J_x^Q(d)$ is replaced by the electric current $J_x^e(d)$, and the thermal resistivities ρ_{Th} are replaced by the electric resistivities. The electrical counterpart of the shunt effect in Fig. 12(b) is obtained without adjustable parameter by the gray line. It can be noticed that the reproducibility from one sample to the other is much better in the case of electric contact due to the absence of leaks in the electric current.

IV. CONCLUSION

While injecting a longitudinal heat current J_x^Q in ferromagnets, we have observed a transverse voltage ΔV_y that depends on the magnetization states of the permalloy layer. It is shown that this angular dependance follows the characteristic laws of anisotropic Righi-Leduc effect [6]. Indeed, the specific dependence to the magnetization states (θ,φ), the linear dependence to the heat power, and the dependence to the thermocouple ΔS follow the behavior expected for the anomalous and planar Righi-Leduc effects. The signal ΔV_y is then due to a transverse temperature difference $\Delta T(\theta,\varphi)$ that depends on the magnetization direction (θ,φ). The difference ΔT is of the order of 10 mK.

The dominant contribution of anisotropic Righi-Leduc effect has been demonstrated through the role of the thermocouple composed of Bi electrode. However, a significant contribution from the anomalous and planar Nernst effect could be superimposed to the measured anisotropic Righi-Leduc effect. A more systematic and quantitative study of the respective contributions of anisotropic Nernst and anisotropic Righi-Leduc effects remains to be performed.

In conclusion, the magnetovoltaic signal measured in our sample is associated to the planar and anomalous Righi-Leduc effect. Both planar and anomalous Righi-Leduc effects are due to the anisotropy of the system. The two contributions should be *a priori* present in all ferromagnetic materials, being *metallic or insulating*, in the same manner as anomalous and planar Hall effects can be expected in any ferromagnetic conductors. From that point of view, the anomalous Righi-Leduc effect should be related to the so-called magnon-Hall effect.

ACKNOWLEDGMENTS

Financial funding from RTRA Triangle de la physique Projects DEFIT 2009-075T and DECELER 2011-085T, the DGA Projects CAPMAG and SPIN CNV 2146, the FEDER, France, La région Lorraine, Le grand Nancy, ICEEL, and the ANR-12-ASTR-0023 Trinidad is greatly acknowledged.

[1] A. Leduc, Modifications de la conductibilité calorifique du bismuth dans un champ magnétique, J. Phys. Theor. Appl. **7**, 519 (1888).
[2] E. H. Hall, Measurement of the four magnetic transverse effects, Phys. Rev. **26**, 820 (1925).
[3] R. Karplus and J. M. Luttinger, Hall effect in ferromagnetics, Phys. Rev. **95**, 1154 (1954).
[4] N. Nagasoa *et al.*, Anomalous Hall effect, Rev. Mod. Phys. **82**, 1539 (2010).
[5] T. R. McGuire and R. I. Potter, Anisotropic magnetoresistance in ferromagnetic 3d alloys, IEEE Trans. Mag. **11**, 1018 (1975).
[6] J.-E. Wegrowe, D. Lacour, and H.-J. Drouin, Anisotropic magnetothermal transport and spin Seebeck effect, Phys. Rev. B **89**, 094409 (2014).
[7] L. Onsager, Reciprocal relations in irreversible processes, II, Phys. Rev. **38**, 2265 (1931).
[8] K. Tanabe *et al.*, Observation of magnon Hall-like effect for sample-edge scattering in unsaturated YIG, Phys. Stat. Solidi B1 **253**, 783 (2016).
[9] S. Fujimoto, Hall Effect of Spin Waves in Frustrated Magnets, Phys. Rev. Lett. **103**, 047203 (2009).
[10] H. Katsura, N. Nagaosa, and P. A. Lee, Theory of the Thermal Hall Effect in Quantum Magnets, Phys. Rev. Lett. **104**, 066403 (2010).
[11] R. Matsumoto and S. I. Murakami, Theoretical Prediction of a Rotating Magnon Wave Packet in Ferromagnets, Phys. Rev. Lett. **106**, 197202 (2011).
[12] T. Qin, Q. Nui, and J. Shi, Energy Magnetization and the Thermal Hall Effect, Phys. Rev. Lett. **107**, 236601 (2011).
[13] Y. Onose *et al.*, Observation of the magnon Hall effect, Science **329**, 297 (2010).
[14] T. Ideue, Y. Onose, H. Katsura, Y. Shiomi, S. Ishiwata, N. Nagaosa, and Y. Tokura, Effect of lattice geometry on magnon Hall effect in ferromagnetic insulators, Phys. Rev. B **85**, 134411 (2012).
[15] J. Kimling, J. Gooth, and K. Nielsch, Anisotropic magnetothermal resistance in Ni nanowires, Phys. Rev. B **87**, 094409 (2013).
[16] S. Y. Huang, W. G. Wang, S. F. Lee, J. Kwo, and C. L. Chien, Intrinsic Spin-Dependent Thermal Transport, Phys. Rev. Lett. **107**, 216604 (2011).
[17] A. D. Avery, M. R. Pufall, and B. L. Zink, Determining the planar Nernst effect from magnetic-field-dependent thermopower and resistance in nickel and permalloy thin films, Phys. Rev. B **86**, 184408 (2012).
[18] A. D. Avery, M. R. Pufall, and B. L. Zink, Observation of the Planar Nernst Effect in Permalloy and Nickel Thin Films with in-Plane Thermal Gradients, Phys. Rev. Lett. **109**, 196602 (2012).

[19] H. Schultheiss, J. E. Pearson, S. D. Bader, and A. Hoffmann, Thermoelectric Detection of Spin Waves, Phys. Rev. Lett. **109**, 237204 (2012).

[20] M. Schmid, S. Srichandan, D. Meier, T. Kuschel, J.-M. Schmalhorst, M. Vogel, G. Reiss, C. Strunk, and C. H. Back, Transverse Spin Seebeck Effect Versus Anomalous and Planar Nernst Effects in Permalloy Thin Films, Phys. Rev. Lett. **111**, 187201 (2013).

[21] D. Meier, D. Reinhardt, M. Schmid, C. H. Back, J. M. Schmalhorst, T. Kuschel, and G. Reiss, Influence of heat flow directions on Nernst effects in Py/Pt bilayers, Phys. Rev. B **88**, 184425 (2013).

[22] C. T. Bui and F. Rivadulla, Anomalous and planar Nernst effects in thin films of the half-metallic ferromagnet $La_{2/3}Sr_{1/3}MnO_3$, Phys. Rev. B **90**, 100403 (2014).

[23] K. Uchida *et al.*, Observation of the spin Seebeck effect, Nature (London) **455**, 778 (2008).

[24] J. Flipse, F. K. Dejene, D. Wagenaar, G. E. W. Bauer, J. B. Youssef, and B. J. van Wees, Observation of the Spin Peltier Effect for Magnetic Insulators, Phys. Rev. Lett. **113**, 027601 (2014).

[25] L. J. Cornelissen *et al.*, Long-distance transport of magnon spin information in a magnetic insulator at room temperature, Nat. Phys. **11**, 1022 (2015).

[26] Y. Niimi, M. Morota, D. H. Wei, C. Deranlot, M. Basletic, A. Hamzic, A. Fert, and Y. Otani, Extrinsic Spin Hall Effect Induced by Iridium Impurities in Copper, Phys. Rev. Lett. **106**, 126601 (2011).

[27] K. Harii *et al.*, Inverse spin-Hall effect and spin pumping in metallic films, J. Appl. Phys. **103**, 07F311 (2008).

[28] S. Y. Huang, X. Fan, D. Qu, Y. P. Chen, W. G. Wang, J. Wu, T. Y. Chen, J. Q. Xiao, and C. L. Chien, Transport Magnetic Proximity Effects in Platinum, Phys. Rev. Lett. **109**, 107204 (2012).

[29] H. Nakayama, K. Ando, K. Harii, T. Yoshino, R. Takahashi, Y. Kajiwara, K. Uchida, Y. Fujikawa, and E. Saitoh, Geometry dependence on inverse spin Hall effect induced by spin pumping in $Ni_{81}Fe_{19}$/Pt films, Phys. Rev. B **85**, 144408 (2012).

[30] M. Althammer, S. Meyer, H. Nakayama, M. Schreier, S. Altmannshofer, M. Weiler, H. Huebl, S. Geprags, M. Opel, R. Gross, D. Meier, C. Klewe, T. Kuschel, J. M. Schmalhorst, G. Reiss, L. Shen, A. Gupta, Y. T. Chen, G. E. W. Bauer, E. Saitoh, and S. T. B. Goennenwein, Quantitative study of the spin Hall magnetoresistance in ferromagnetic insulator/normal metal hybrids, Phys. Rev. B **87**, 224401 (2013).

[31] V. Castel *et al.*, Platinum thickness dependence of the inverse spin-Hall voltage from spin pumping in a hybrid yttrium iron garnet/platinum system, Appl. Phys. Lett. **101**, 132414 (2012).

[32] W. J. Xu *et al.*, Scaling law of anomalous Hall effect in Fe/Cu bilayers, Eur. Phys. J. B **65**, 233 (2008).